Journal of
Instrumentation

Analysis of neutron related background of the SXR GEM diagnostic on MAST-U

Published by IOP Publishing for Sissa Medialab

Received: *January 16, 2025*
Accepted: *April 5, 2025*
Published: *May 7, 2025*

7th International Conference Frontiers in Diagnostic Technologies
INFN research center of Frascati, Italy
21–23 October 2024

Analysis of neutron related background of the SXR GEM diagnostic on MAST-U

A. Celora[a,*] **F. Guiotto**[b,c] **F. Caruggi**[a,d] **S. Cancelli**[a,e] **G. Claps**[f,g] **F. Cordella**[f,g] **V. de Leo**[f,g] **L. Garzotti**[h] **G. Grosso**[e] **E. Lazzaro**[e] **D. Pacella**[f,g] **O. Putignano**[d,e] **E. Rose**[h] **R. Sarwar**[h] **R. Scannell**[h] **M. Tardocchi**[a,d,e] **G. Croci**[a,d,e] **A. Muraro**[d,e] **and the MAST-U team**[1]

[a] *Dipartimento di Fisica "G. Occhialini", University of Milano-Bicocca, Piazza della Scienza 3, Milano, Italy*
[b] *Centro Ricerche Fusione (CRF) - University of Padova, C.so Stati Uniti 4, 35127, Padova, Italy*
[c] *Consorzio RFX (CNR, ENEA, INFN, University of Padova, Acciaierie Venete SpA), C.so Stati Uniti 4, 35127, Padova, Italy*
[d] *INFN, Sezione Milano-Bicocca, Piazza della Scienza 3, Milano, Italy*
[e] *Istituto per la Scienza e Tecnologia dei Plasmi, CNR, via Cozzi 53, Milano, Italy*
[f] *ENEA-Frascati, V.E. Fermi 44, Frascati, Italy*
[g] *INFN, Laboratori Nazionali di Frascati, via Enrico Fermi 40, Frascati, Italy*
[h] *UKAEA (United Kingdom Atomic Energy Authority), Culham Campus, Abingdon, Oxfordshire, OX14 3DB, U.K.*

E-mail: a.celora@campus.unimib.it

Abstract: Soft X-Ray (SXR) diagnostics are crucial in magnetically confined nuclear fusion experiments for studying plasma behavior, such as magneto-hydrodynamic (MHD) instabilities and impurity dynamics. Gas Electron Multiplier (GEM) detectors offer a valuable approach for SXR detection, given their radiation hardness and unique combination of high-rate imaging and spectroscopic capabilities. This study investigates the impact of high neutron rate on the GEM detector spectroscopic response in the MAST-U spherical tokamak. A sample energy spectrum obtained from the GEM diagnostic is compared with Geant4 simulations of both SXR and neutron sources to characterize background effects and study the detector response.

Keywords: Detector modelling and simulations I (interaction of radiation with matter, interaction of photons with matter, interaction of hadrons with matter, etc); Micropattern gaseous detectors (MSGC, GEM, THGEM, RETHGEM, MHSP, MICROPIC, MICROMEGAS, InGrid, etc); Plasma diagnostics - interferometry, spectroscopy and imaging; X-ray detectors

*Corresponding author.
[1] See author list of Harrison et al., *Nucl. Fusion* **59** (2019) 112011.

https://doi.org/10.1088/1748-0221/20/05/C05010

Contents

2025 JINST 20 C05010

1 Introduction

In magnetic confinement fusion experiments, Soft X-Ray (SXR) emissions, in the range 1 to 20 keV, provide crucial data on key plasma parameters like electron temperature, magneto-hydrodynamics instabilities and impurity levels and therefore SXR diagnostics are widely employed in tokamak machines. Gas Electron Multiplier [1] (GEM) detectors are increasingly used as SXR diagnostics [2–4] due to their radiation hardness and ability to combine high-rate imaging with spectroscopic capabilities [5].

The GEM detector described in section 1.1 was installed on the MAST-U tokamak [6] during the 2023 experimental campaign [7]. MAST-U is a spherical tokamak characterized by its compact design and enhanced β performance. However, the compact design results in higher neutron rate on detector, posing challenges due to intense neutron background. This work presents the energy spectrum of an illustrative shot and compares it with Geant4 [8] simulations to assess neutron-related background effects.

1.1 The GEM detector

The GEM detector used in this work has a standard triple GEM configuration with Aluminum GEM foils. The interacting gas is an $ArCO_2$ 70–30% mixture. In front of the cathode, made of a 12.5µm aluminated mylar film, there is a 6 mm gap filled with $ArCO_2$ 70–30%. The sensitive volume is a gap after the cathode, 4 mm thick, followed by the first GEM foil. The read-out anode of the detector is a matrix of 16x16 6mm^2 square pixels, where each pixel is connected to a single channel of the electronic readout. The electronics system is composed by a set of Application Specific Integrated Circuits (ASICs) called GEMINI [9] paired with a custom made Field Programmable Gate Array. This allows independent photon counting mode on each pixel, to obtain time and energy information by exploiting the Time over Threshold (ToT) technique [10]. The detector characterization and energy calibration is described in [11].

1.2 Experimental set-up

The GEM detector installed on MAST-U measures $10 \times 10 \times 3$ cm^3 and is housed in an aluminum casing for electromagnetic interference (EMI) protection. Positioned with a radial point of view in a pinhole configuration, it is located about 26 cm outside of the tokamak vacuum chamber, thus 2.7 m from the tokamak center. Thus the solid angle subtended by the detector with respect to the center of the tokamak is therefore $\Omega_{\text{det}} = (0.1\text{m})^2/(2.7\text{m})^2 = 1.37 * \cdot 10^{-3}$sr. A schematic vertical section of the tokamak and installed detector is shown in figure 1. The vacuum port features a circular 25 µm thick Beryllium window with a 13 mm diameter. A circular aperture, with a diameter of 1 mm, is positioned one centimeter beyond the Beryllium window, forming the pinhole. 3D-printed plastic components are installed around the detector window and the Beryllium window to provide both mechanical and electrical protection from accidental external access. The set-up is shown in the schematics in figure 1 and in the CAD model in figure 2. Table 1(a) indicates the materials of the main set-up components. And table 1(b) lists the materials on the SXR path, from the plasma, to the detector sensitive volume.

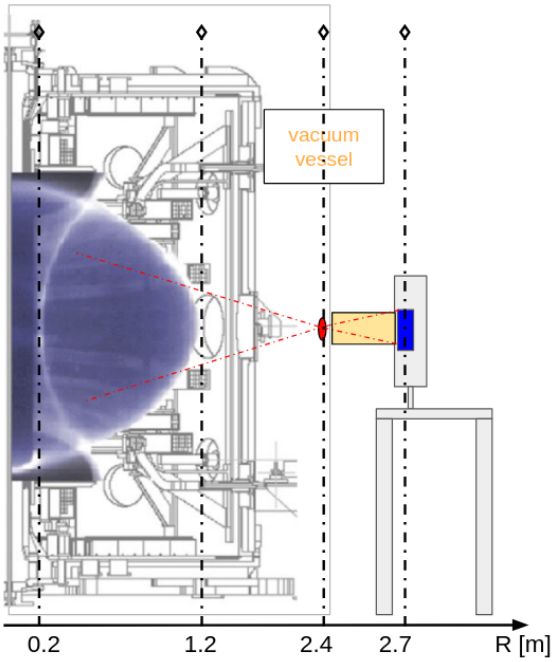

Figure 1. Schematic vertical section of the GEM diagnostic installation on MAST-U. The GEM integration scheme is overlaid on the MAST-U schematic from [12], showing a typical plasma cross-section. The detector (blue rectangle) is enclosed in its EMI shielding case, with plastic protection (yellow) for the GEM cathode and beryllium windows (red ellipse, not to scale). The camera view cone is marked by red dashed lines, while vertical dashed lines indicate the radial positions of the central column surface, first wall, vacuum vessel outer surface, and GEM detector. Adapted from [12]. CC BY 4.0.

2 Set-up simulation

In addition to the SXR signal, the GEM detector is exposed to a significant neutron flux. A first-order geometrical estimate (detailed in section 3) suggests that during an H-mode plasma, the total number of neutrons incident on the entire surface of the detector (100cm^2) is approximately

2025 JINST 20 C05010

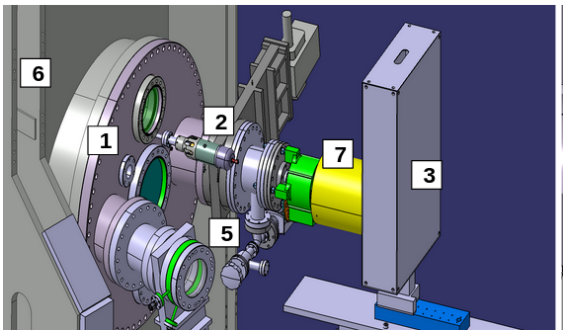

(a) CAD model view.

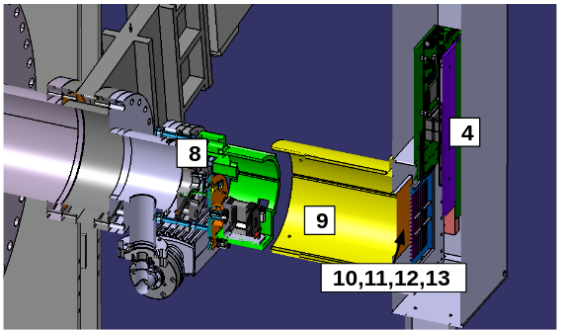

(b) Section of the CAD model.

Figure 2. CAD model of the GEM diagnostic integrated on MAST-U. Labels are used to individuate the main components of the setup, described in tables 1(a) and 1(b).

Table 1. Summary of key materials in the experimental setup. Table (a) Lists surrounding components contributing to neutron background. Table (b) Details the materials and thicknesses along the SXR path from plasma to the detector.

Surrounding Elements	Material	Label
Tokamak flange	Stainless Steel	1
GEM Port	Stainless Steel	2
GEM EMI box	Aluminum	3
Detector structure	FR4	4
Valve supports	Stainless Steel	5
Vacuum chamber wall	Stainless Steel	6
Protection	Plastic (PLA)	7

(a) List of the key elements of the experimental setup that contribute to neutron-related background, along with their respective materials and labels as referenced in the CAD scheme of figure 2.

SXR Path element	Thickness	Label
Plasma	1.2 m	
Vacuum	1.2 m	
Beryllium window	25 µm	8
Air	26 cm	9
Aluminized Mylar window	12.5 µm	10
$ArCO_2$	6 mm	11
Aluminized Mylar cathode	12.5 µm	12
$ArCO_2$ detector volume	4 mm	13

(b) Materials traversed by photons along the SXR path and their respective lengths. Ordered from the plasma source to the detector sensitive volume.

$\Phi_{det} = 10^9$n/s. Therefore the detector response to SXR and the impact of neutron radiation on its performance have been investigated using Geant4 simulations to assess sensitivity to neutron-related background and its influence on measurements. The simulation geometry is imported into Geant4 from a CAD model developed to integrate the GEM detector and its support structure within the MAST-U tokamak (see figure 2).

In the experiments, SXR radiation from the extended plasma volume is collimated by the pinhole and flange system, whereas neutrons can reach the detector both directly and after scattering off tokamak components. In the Geant4 simulations, these radiation sources are modeled as particle beams, originating from the center of the plasma, each consisting of $5 \cdot 10^8$ particles emitted from the tokamak center and directed at the detector in separate simulation runs. The beam cross-section is made larger than the tokamak flange to account for radiation interactions within the flange and materials.

While this beam assumption is accurate for SXR radiation, it represents an oversimplification for neutrons. Neutrons that are not initially directed toward the detector may still reach it through scattering interactions with tokamak components. As a result, this method provides only a first-order

2025 JINST 20 C05010

approximation and does not fully account for the complexities of neutron transport within the tokamak. Nonetheless, it offers a practical approach to understanding the neutron-induced background in the GEM detector. A more precise evaluation of the effective detector acceptance would require simulating a volumetric neutron source within a complete tokamak model, incorporating all relevant scattering processes. However, such an approach would necessitate specialized tools and extensive calibration efforts, which fall outside the scope of this study.

Neutrons in the simulations are generated with an energy of 2.45 MeV, corresponding to deuterium-deuterium (D-D) fusion products. The soft X-ray (SXR) emission spectrum in MAST-U plasmas is primarily governed by Bremsstrahlung radiation from a Maxwellian plasma [13].The Bremsstrahlung emission at a defined energy E, as a function of position $\bar{x}$ within the plasma and time t, is given by:

$$\epsilon_{\text{Brem}}(E,\bar{x},t) \propto E \cdot n_e(\bar{x},t)^2 \cdot T_e(\bar{x},t)^{-1/2} \exp\left[\frac{-E}{k_B T_e(\bar{x},t)}\right] \tag{2.1}$$

For the conditions considered in this study, the electron temperature is set to $T_e = 1\text{keV}$, and the normalized electron density is $n_e = 1\text{m}^{-3}$. Particles that deposit energy in the detector sensitive volume are monitored, in term of deposited energy, interaction process and volume in which they were created, to assess signal and neutron-related background generation. The simulations use multiple physics lists: "QGSP-BIC-HP" physics list for hadronic processes; "G4IonPhysicsXS" and "G4IonElasticPhysics" for ion scattering; "G4EmPenelopePhysics" for Electromagnetic interactions; Fluorescence, Auger Process and Particle Induced X-ray are also activated to accurately capture photon interaction.

3 Analysis of the energy spectrum for an LH mode transition observed at MAST-U

In [7] the presence of a neutron-related background signal in the GEM time trace has been shown. This work analyzes the neutron related background in the GEM energy spectrum, which limits the diagnostic spectroscopic potential. The MAST-U shot #49325 provides a clear example of the effect of such background and is the focus of the analysis.

The GEM data are interpreted by comparison with a selection of MAST-U diagnostic data (shown in figure 3). In figure 3(a) the Plasma Current, in the first row, asses the overall plasma status. The Neutral Beam Injection (NBI) power output measure, in the second line, indicates the status of the heating system. The fission chambers diagnostic provides the total neutron emission from the tokamak ϵ_n at 4π, shown in the third line. The SXR camera current signal, in the fourth line, shows the current signal of the diodes camera produced by SXR emission integrated in the core region of the plasma. The electron temperature and density of the plasma core, measured by the Thomson Scattering diagnostic are shown in figure 3(b).

In this shot, Neutral Beam Injection (NBI) heating was activated at 0.46 s. Therefore, the shot can be divided into two halves. The first half is characterized by a pure Ohmic plasma, in L mode, exhibiting a realtively low neutron production, with the MAST-U fission chambers [14] recording a total neutron emission rate of 10^{11}n/s.

In a first-order geometrical approximation, the total neutron emission can be assumed to originate from the tokamak center and be emitted isotropically. This provides a rough estimate of the neutron rate on the detector surface: $\Phi_{\text{det}} \approx \frac{\epsilon_n \cdot \Omega_{\text{det}}}{4\pi} \approx 10^7$n/s, where Ω_{det} is the solid angle subtended by the detector (see section 1.2), and ϵ_n represents the total neutron emission. The second half presents a beam-heated plasma, in H mode, in which the neutron total emission grows by two orders of magnitude,

2025 JINST 20 C05010

for an approximated incident neutron rate on the detector of $\Phi_{det} \approx 10^9$n/s. This change leads to a sudden appearance of the high-energy tail in the GEM energy spectrogram, as seen in figure 4(a), and is also reflected in the spectra differences shown in figure 4(b).

The simulated SXR reference spectrum of the configuration, with an electron temperature of 1 keV, is shown in figure 5. The shape of the simulated spectrum aligns only with the GEM spectrum of the Ohmic plasma: photons with energies below 3.2 keV are absorbed by the air in front of the detector, and the exponential decay is a result of the electron temperature's influence on the Bremsstrahlung emission. The cause of the shape difference in the low range, namely before 4 keV, can be found in the non linearity of the GEM energy calibration which distort the spectrum. Instead, the high energy tail of the recorder spectrum in H mode cannot be explained by the SXR radiation, but by neutron background, as shown in section 4.

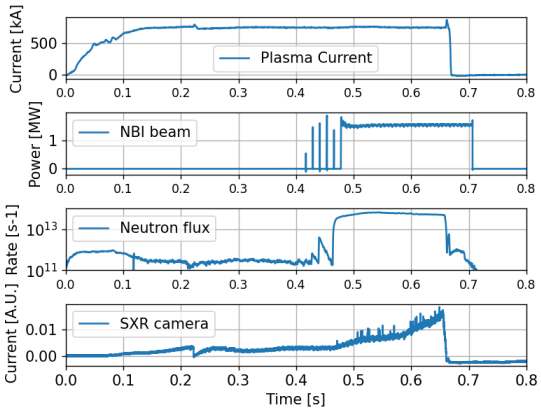

(a) Time evolution of key plasma parameters: (from top to bottom) plasma current, injected NBI power, total measured neutron emission, and SXR signal from a central chord of the MAST-U horizontal camera.

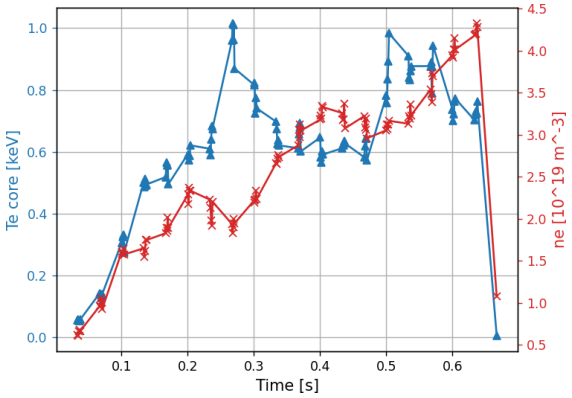

(b) Time evolution of the electron temperature and density in the core region, measured by the Thomson Scattering diagnostic.

Figure 3. MAST-U diagnostics data, shot #49325.

3.1 GEM timetrace analysis

The GEM energy spectrogram in figure 4(a) reveals a sudden appearance of the high-energy tail, in contrast to the gradual increase observed in the SXR signal detected by the MAST-U SXR camera (figure 3(a)). This can be explained by the differences in the intrinsic energy sensitivities of the diagnostics: the GEM diagnostic, in the current setup, is sensitive to photons above 3 keV, while the diodes are optimized for detection from 1 keV [15]. Moreover, the radiation absorption along the two diagnostic lines of sight differs: the diodes are located in the tokamak vacuum chamber, while the GEM detector is positioned outside of it, creating a 26 cm air absorption path that limits the detection of low-energy photons.

To analyze the GEM time trace, it is compared to an estimated time-resolved SXR emissivity, $\epsilon_{SXR}(t)$, calculated using a custom Python script. The core plasma electron density and temperature, obtained from Thomson scattering data (figure 3(b)), are used in equation (2.1) to determine the SXR emissivity from the core at different energies and time $\epsilon_{Brem}(E,t)$. Soft X-ray absorption along the photon path (see table 1(b)) is accounted for by applying an energy-dependent absorption factor. This

2025 JINST 20 C05010

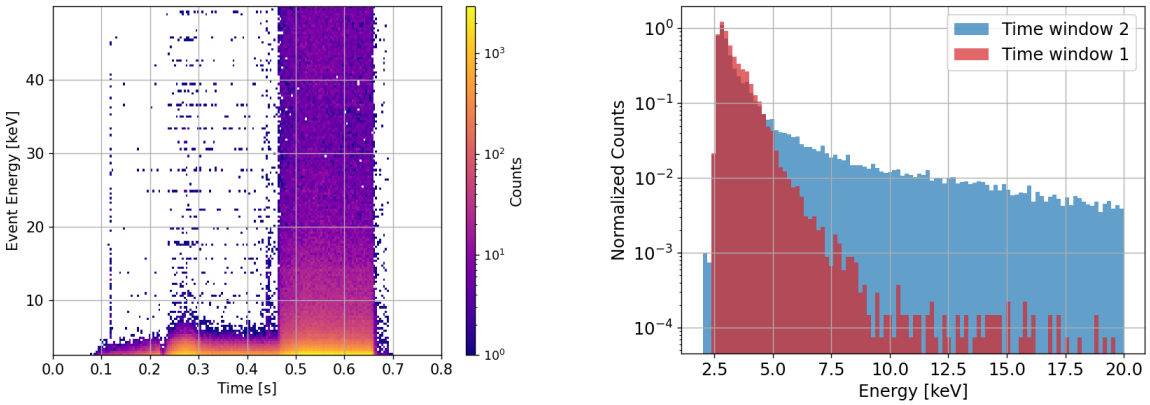

(a) Energy spectrogram obtained with the GEM detector. On the x-axis the time (time binning of 1 ms), on the y-axis the SXR energy in keV and the color proportional to the logarithmic number of events per bin.

(b) Experimental normalized energy spectra from the GEM camera in different time windows: Time window 1 (up to 0.45 sec) and Time window 2 (starting from 0.46 sec).

Figure 4. MAST-U shot #49325, GEM data.

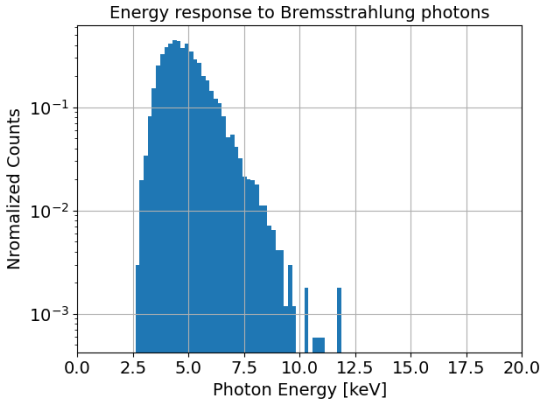

Figure 5. Simulated SXR spectrum for the GEM experimental setup and a MAST-U electron temperature of 1 keV.

factor incorporates the absorption coefficient, $\mu_{\text{mat}}(E)$, of each material and the corresponding path length, l_{mat}. The total emissivity at each time step is then obtained by summing the emissivity at different energies. The calculations can be summarized in the following equation:

$$\epsilon_{\text{SXR}}(t) = \sum_{E=E_{\text{min}}}^{E_{\text{max}}} \left[\epsilon_{\text{Brem}}(E, T_e(\text{core}, t), n_e(\text{core}, t)) \cdot \prod_{\text{mat}} e^{-\mu_{\text{mat}}(E)\cdot l_{\text{mat}}} \right] \tag{3.1}$$

The results, presented in figure 6(a), indicate that when selecting GEM photons with energies below 7 keV, the time trace closely follows the SXR estimation. Conversely, when considering only photons with energies above 7 keV, the GEM time trace aligns with the fission chamber's response to the neutron emission, as in figure 6(b). This highlights the influence of neutron-related background on the high-energy portion of the spectrum and demonstrates the potential for distinguishing this contribution.

2025 JINST 20 C05010

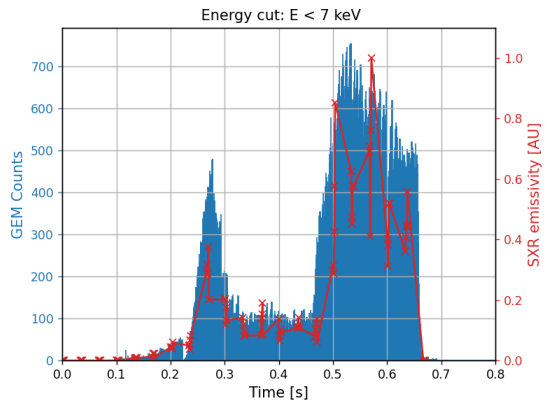

(a) Comparison between the GEM time trace, with 1 ms time binning, for energy between 3 and 7 keV (filled blue signal); and the estimated SXR emission $\epsilon_{SXR}(t)$ (red line with cruxes points).

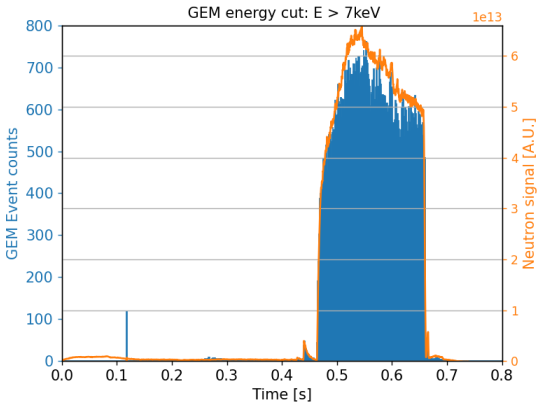

(b) Comparison between the GEM time trace, with 1 ms time binning, for energy above 7 keV (filled blue signal), and the fission chamber neutron total emission (orange curve).

Figure 6. MAST-U shot #49325. Comparison of GEM timetrace, estimated SXR emissivity, and fission chamber neutron total emission.

4 Neutron background simulation

The main results of the neutron beam simulations are shown in figure 7(a). It is observed that the main families of particles that deposit background energy in the GEM sensitive area, in the energy range of interest (1–20 keV) are electrons and neutrons. The genesis of the interacting electrons can be traced through the simulation: neutrons scatter on the materials on their path, emit secondary gamma particles, which subsequently interact through Compton scattering with other diagnostic surrounding components, resulting in electrons that enter the detector sensitive volume. The volumes where the secondary gamma and electrons are generated are shown in figure 7(b). Secondary sources of deposited energy are incident gamma particles and protons caused by the interaction of neutrons on the cathode. The interactions labeled as "Neutrons" in figure 7 are caused by ions created from neutron scattering with the active gas medium.

The simulated spectrum closely matches the GEM energy spectrum from the high-neutron region of shot #49325, shown as the blue curve in figure 4(b). To confirm this, both spectra are normalized on the total area, and their energy tails (20–40 keV) are fitted with an exponential function, $y = A \cdot e^{-E/\tau}$. The decay constants agree within a sigma: ($\tau_{sim} = 31.97 \pm 3.90$) keV and ($\tau_{meas} = 27.42 \pm 1.60$) keV. The superposed spectra are shown in figure 8.

While the exponential fits confirm statistical compatibility in the high-energy tails, the simulated spectrum shows a stronger high-energy component. This is because it represents only neutron induced events, whereas the experimental spectrum includes both SXR and neutron contributions, with SXR dominating between 2.5 and 10 keV.

5 Conclusions

This study investigates neutron-induced background effects on SXR detection in the MAST-U tokamak using a GEM diagnostic, with a focus on energy spectrum analysis. The results highlight that, while neutron-related interference can impact the spectroscopic capabilities of the GEM diagnostic

2025 JINST 20 C05010

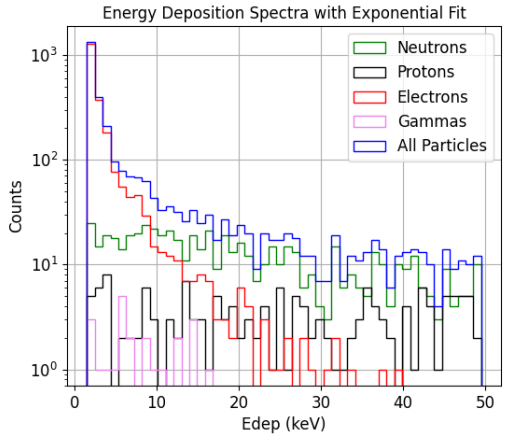

(a) Spectrum of Energy deposited in the GEM sensitive volume, divided by interacting entering particle.

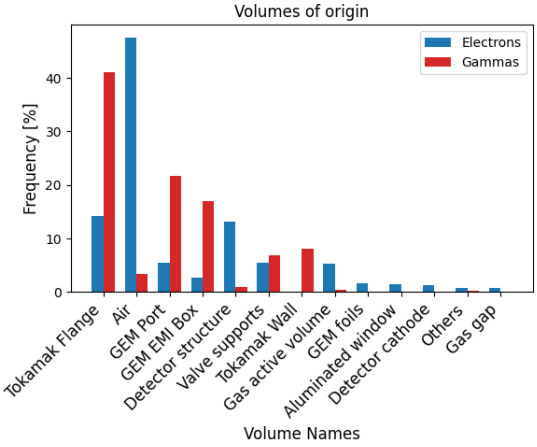

(b) List of Mother Volumes of the electrons that deposit energy in the GEM detector and of the gamma particles that produce them.

Figure 7. Geant4 simulation of the GEM response to 2.5 MeV neutron beam in the present setup, and list of Source Volumes contributing to the GEM detector energy deposition.

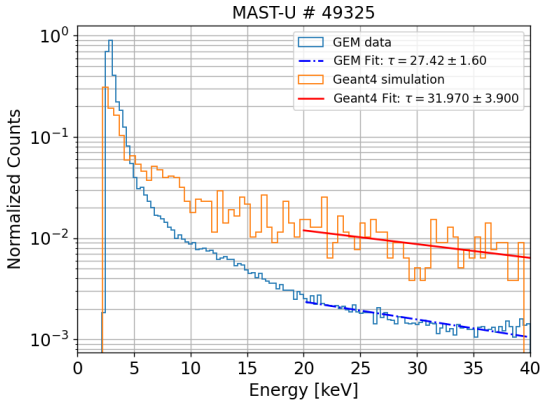

Figure 8. Superposition of the GEM spectrum for the MAST-U shot #49325 for t > 0.46 sec, and of the Geant4 neutron simulated spectrum with corresponding fit lines.

for total neutron emission from the tokamak higher than 10^{12}n/s, its influence on photon-counting capabilities remains marginal, and can be minimized by offline energy threshold analysis. Moreover, in Ohmic-heated shots, the impact is significantly reduced across both spectroscopic and photon-counting aspects due to the smaller neutron rate on the detector.

The study identifies the primary source of neutron background as interactions with surrounding materials, such as the tokamak outer wall, which are inherent to the system's operation. These findings emphasize the importance of targeted strategies to mitigate background noise, thereby enhancing the diagnostic's signal-to-noise ratio and improving its spectroscopic performance.

As potential pathways for optimization, the authors propose the use of a helium gas buffer to reduce SXR attenuation and a $NeCO_2$ gas mixture to enhance low-energy SXR detection efficiency, particularly in the 2–3 keV range. These strategies will be explored in future research to further improve the diagnostic's performance.

2025 JINST 20 C05010

Acknowledgments

This work has been carried out within the framework of the EUROfusion Consortium, funded by the European Union via the Euratom Research and Training Programme (Grant Agreement No 101052200 — EUROfusion) and from the EPSRC [grant number EP/W006839/1]. Views and opinions expressed are however those of the author(s) only and do not necessarily reflect those of the European Union or the European Commission. Neither the European Union nor the European Commission can be held responsible for them.

References

[1] F. Sauli, *The gas electron multiplier (GEM): Operating principles and applications*, *Nucl. Instrum. Meth. A* **805** (2016) 2.

[2] F. Cordella et al., *Results and performances of X-ray imaging GEM cameras on FTU (1-D), KSTAR (2-D) and progresses of future experimental set up on W7-X and EAST Facilities*, 2017 *JINST* **12** C10006.

[3] E. Li et al., *First results of the 2D gas electron multiplier in the dominant electron heating scenario on EAST*, *Nucl. Fusion* **59** (2019) 106030.

[4] D. Mazon et al., *First GEM measurements at WEST and perspectives for fast electrons and heavy impurities transport studies in tokamaks*, 2022 *JINST* **17** C01073.

[5] A. Muraro et al., *Development and characterization of a new soft x-ray diagnostic concept for tokamaks*, 2019 *JINST* **14** C08012.

[6] W. Morris et al., *MAST Upgrade Divertor Facility: A Test Bed for Novel Divertor Solutions*, *IEEE Trans. Plasma Sci.* **46** (2018) 1217.

[7] A. Celora et al., *Assessment of a space and energy resolved diagnostic based on GEM technology on MAST-U*, *Meas. Sci. Technol.* **36** (2024) 016019.

[8] GEANT4 collaboration, *GEANT4 — A Simulation Toolkit*, *Nucl. Instrum. Meth. A* **506** (2003) 250.

[9] A. Pezzotta et al., *GEMINI, a CMOS 180 nm mixed-signal 16-channel ASIC for Triple-GEM detectors readout*, in the proceedings of the *IEEE SENSORS 2015*, Busan, Korea (South) (2015), p. 1–4 [DOI:10.1109/ICSENS.2015.7370468].

[10] S. Cancelli et al., *Electronic readout characterisation of a new soft X-ray diagnostic for burning plasma*, 2022 *JINST* **17** C08028.

[11] F. Caruggi et al., *Performance of a triple GEM detector equipped with Al-GEM foils for X-rays detection*, *Nucl. Instrum. Meth. A* **1047** (2023) 167855.

[12] V.F. Shevchenko et al., *Long Pulse EBW Start-up Experiments in MAST*, *EPJ Web Conf.* **87** (2015) 02007.

[13] S. Von Goeler et al., *Thermal X-ray spectra and impurities in the ST Tokamak*, *Nucl. Fusion* **15** (1975) 301.

[14] C. Vincent et al., *Fission chamber data acquisition system for neutron flux measurements on the Mega-Amp Spherical Tokamak Upgrade*, *Rev. Sci. Instrum.* **93** (2022) 093509.

[15] M. Anton, M.J. Dutch and H. Weisen, *Relative calibration of photodiodes in the soft-x-ray spectral range*, *Rev. Sci. Instrum.* **66** (1995) 3762.

2025 JINST 20 C05010